Accepted for presentation in: IEEE International Symposium on Measurement in Networking and Communications (MNC), Naples, Italy, July 2026

Two Birds, One Stone: FR3 as 6G Golden Band? Analysis from Measurement-Calibrated Ray Tracing

Marco Danger, Stefan Böcker, and Christian Wietfeld
Communication Networks, TU Dortmund University, 44227 Dortmund, Germany
E-mail: {Marco.Danger, Stefan.Boecker, Christian.Wietfeld}@tu-dortmund.de

***Abstract*—Future 6G networks must support highly heterogeneous services with conflicting requirements in coverage, capacity, link stability, and deployment efficiency. The established frequency ranges, Frequency Range 1 (FR1) and FR2, represent two operational extremes, providing either wide area robustness or very high peak data rates, thereby exposing the fundamental trade-off between coverage and performance. The upper mid-band, FR3 (7 GHz to 24 GHz), has therefore attracted growing interest as an intermediate solution. This work develops a measurement-calibrated ray tracing framework based on extensive FR1 and FR2 measurements in a large-scale industrial environment, enabling cross-frequency predictions for FR3 with a propagation modeling error between 3.11 dB and 4.79 dB (RMSE). Furthermore, a device-specific mapping from received power to achievable data rate is derived from the measurement data, enabling consistent performance comparison across FR1, 2, and 3. The results highlight frequency-specific trade-offs, showing that FR3 balances coverage and capacity effectively in the considered industrial indoor scenario. In a second, highly cluttered warehouse environment, coverage evaluated at 99 % of the configuration-dependent maximum Uplink (UL) data rate reveals that FR3 exhibits favorable infrastructure scaling behavior, requiring fewer transmitters than FR2 while enabling higher data rates than FR1. These findings indicate that FR3 can appropriately be referred to as 6G golden band, achieving an efficient balance between coverage and capacity. Yet, comprehensive field validation and regulatory guidance on upper mid-band allocation remain crucial to assess its practical viability without compromising existing radio systems.**

***Index Terms*—6G, FR3, ray tracing, measurement-calibrated, cross-band, system-level evaluation.**

I. Introduction

The evolution towards 6G is driven by increasingly diverse and demanding application requirements, ranging from ultra-reliable low-latency control to bandwidth-intensive extended reality and digital twin services [1, 2]. Meeting these heterogeneous demands with a single Frequency Range (FR) is inherently challenging, as different services impose fundamentally conflicting demands on coverage, capacity, link stability, and deployment efficiency. While FR1 (< 7 GHz) provides robust wide-area coverage and stable connectivity, and FR2 (> 24 GHz) enables extreme peak data rates, both represent opposing ends of the coverage–capacity trade-off. Consequently, neither FR alone can efficiently support the full spectrum of envisioned 6G use cases, particularly in complex industrial environments. In this context, the emerging upper mid-band, FR3 (7 GHz to 24 GHz), has gained significant attention as a potential intermediate solution to combine favorable propagation characteristics with substantially increased bandwidth ("*two birds with one stone*") compared to FR1 [3]. This positions FR3 as a promising candidate for addressing the limitations of existing FRs and has led to its characterization as potential *golden band* for future 6G systems.

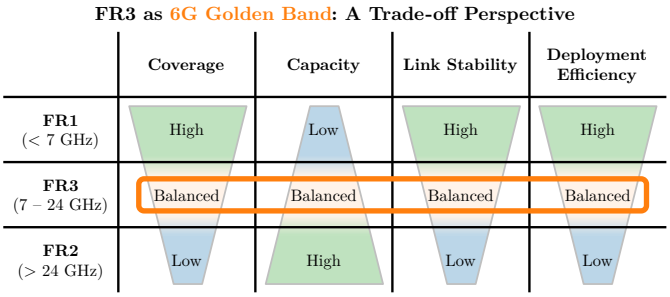

Fig. 1: Qualitative comparison of Frequency Ranges (FRs): The conceptual classification illustrates the balanced characteristics of FR3 across key metrics, motivating its consideration as a potential 6G golden band.

Despite its promising characteristics, the role of FR3 in future 6G systems remains insufficiently understood, particularly with respect to its behavior across different dimensions and deployment scenarios. Therefore, Fig. 1 provides a qualitative comparison of FRs based on key metrics such as coverage, capacity, link stability, and deployment efficiency. The conceptual classification emphasizes the inherent trade-offs of each FR and highlights the comparatively balanced characteristics of FR3 across these dimensions. This observation motivates the systematic, measurement-grounded evaluation of this work to assess whether FR3 can indeed fulfill the role of a *golden band* in practical industrial environments.

Despite its growing relevance, large-scale experimental evaluations of FR3 remain limited due to the scarcity of commercially available systems and deployments. To address those limitations, this work leverages extensive FR1 and FR2 measurements collected in a real industrial environment using commercial mobile User Equipments (UEs). These measurements are used to calibrate frequency-dependent ray tracing simulations within a detailed 3D model of the scenario, enabling cross-frequency propagation predictions for FR3. Based on this measurement-validated framework, the coverage, achievable throughput and link stability of FR1 to 3 are systematically compared under consistent deployment conditions. In addition, the impact of increasing transmitter density on FR-specific target coverage as well as UE data rate is investigated to provide insights into deployment efficiency and scalability across the considered frequencies.

The remainder of this work is structured as follows. In Sec. II, previous studies on the upper mid-band FR3 are reviewed. The methodology is presented in Sec. III, including the employed channel models, the configuration of the frequency-specific as well as measurement-calibrated ray tracing simulations, and the performance prediction. The results are evaluated and discussed in Sec. IV, before the findings and future research directions are summarized in Sec. V.

II. Related Work on FR3 and Multi-Band Systems

The interest in the upper mid-band for future 6G systems has led to increasing research efforts on propagation characterization, channel modeling, and system-level performance evaluation across different FRs, with particular emphasis on the emerging FR3 spectrum. Although dedicated large-scale studies remain limited, recent contributions provide valuable insights into its propagation behavior and deployment potential.

Comprehensive channel measurements in FR3 at 6.75 GHz and 16.95 GHz are reported in [4, 5], where the observed propagation characteristics are compared with existing 3rd Generation Partnership Project (3GPP) channel models. The results show that these models can, in some cases, closely match real-world measurements, as indicated by low Root Mean Square Error (RMSE) values, while in other scenarios notable deviations occur. These findings highlight both the usefulness of such models for initial performance estimation and the need for further refinement based on measurements.

Beyond propagation characterization, several studies have investigated the system-level implications of FR3. In [6], extensive ray tracing simulations were conducted for outdoor and Outdoor to Indoor (O2I) scenarios to investigate FR1, 2, and 3 in terms of performance, coexistence and interference with other radio technologies. Their findings show, among other things, that cross-frequency systems can lead to significant capacity gains. Spectrum coexistence and interference are further discussed in [3, 7] and identified as one of the key challenges of FR3 for 6G. The authors point out that reliable guidelines and ongoing security monitoring are required to avoid compromising existing satellite communications in this frequency band. Furthermore, it is noted that channel models for FR3 already exist (e.g., [8]), but their validity for frequencies between 6 GHz and 24 GHz still requires more extensive experimental verification.

This work utilizes FR1 and FR2 mobile measurements reported in [9], which were obtained in a large-scale industrial indoor environment. These measurements are used to calibrate and refine ray tracing simulations, enabling physically consistent propagation predictions for FR3 that provide more accurate and scenario-specific results than abstract channel models. In addition, based on performance measurements from [9] and [10], a device-specific mapping from simulated received power to achievable data rate is derived for each FR. The resulting analysis provides insights into the capabilities of each individual FR, demonstrates the favorable trade-off between coverage and capacity achieved by FR3, and thereby extends findings reported in earlier studies.

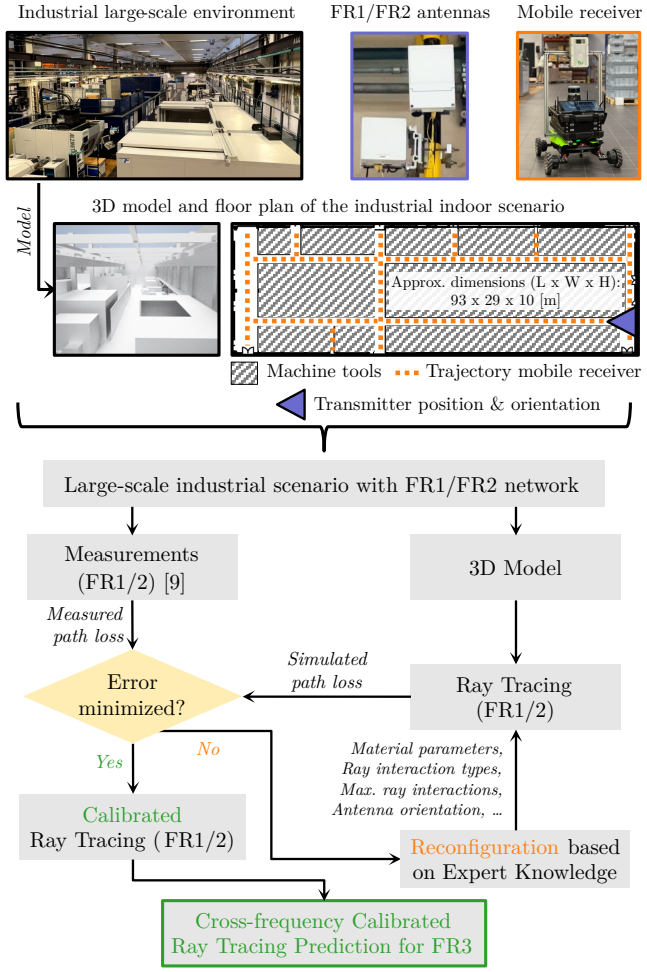

Fig. 2: Radio setup in real industrial environment and framework for calibrated ray tracing to enable cross-frequency propagation prediction for FR3.

III. Measurement-Calibrated Propagation and Performance Prediction Framework

This section presents the methodology used to analyze radio propagation and performance across the considered FRs. First, multiple channel models are introduced, which are used to evaluate the simulation results. Next, the configuration and calibration of the frequency-specific ray tracing simulations are described in detail. Finally, the approach for estimating achievable data rates from received power values is presented, enabling a consistent mapping from physical-layer results to system-level performance.

A. Reference Channel Models for Path Loss Benchmarking

To evaluate the accuracy of the proposed ray tracing framework, its predicted path loss is compared with established stochastic channel models, namely the *WINNER II A1* and *B3* scenarios [11] as well as the *3GPP Indoor Factory (InF)* model defined in [8]. These models are widely used for indoor evaluation and provide a standardized basis for comparison.

The WINNER II A1 and B3 scenarios cover structured indoor environments with partitioned layouts as well as hotspot areas. Although not specifically tailored to industrial facilities, they represent typical indoor propagation assumptions.

In contrast, the 3GPP InF model explicitly targets factory environments and accounts for large halls, clutter, and metallic structures, making it the most relevant standardized reference for industrial deployments. By comparing these stochastic models with a calibrated ray tracing approach, deviations between generic scenario-based assumptions and a deterministic, site-specific model are quantified. This enables an assessment of the extent to which standardized channel models capture realistic industrial propagation conditions.

B. Frequency-specific Ray Tracing Simulation Settings

To enable a frequency-dependent and physically consistent evaluation, multiple ray tracing simulations are conducted using the open-source tool *Sionna RT* [12] and a 3D model of the environment, shown in Fig. 2. Material properties are assigned based on the real-world environment and the material catalog provided by the ray tracing tool: Metallic characteristics are utilized for obstacles, machine tools, walls, and the roof, while concrete is chosen for the floor. To account for non-ideal reflections and unavoidable modeling inaccuracies, the scattering coefficient of all objects is reduced to 0.5 to avoid overly optimistic propagation conditions.

In alignment with the measurement campaign discussed in [9], the network configurations for FR1 and FR2 are replicated in the simulation setup of this work. Following a similar approach as in [6], the antenna array dimensions and system bandwidth are scaled according to the respective carrier frequency, as stated in Tab. I.

The mobile receiver's trajectory, which is marked on the floor plan in Fig. 2, is segmented into 715 individual positions. For each position, the corresponding Channel Impulse Response (CIR) between transmitter and receiver is computed. The simulated FR1 and FR2 results are then compared to the previously introduced path loss models as well as the measured metrics from [9] and, if necessary, simulation parameters are refined to minimize the error between simulated and measured values. This calibration ensures that the propagation conditions are physically validated for extending the analysis to FR3.

C. Data Rate Estimation from Simulated Received Power

Lastly, to compare the performance capabilities of all frequencies within industrial scenarios, the achievable data rate at each receiver position is estimated by combining the calibrated ray tracing results with a device-specific mapping of simulated received power to data rate.

TABLE I: Simulation and data-rate estimation parameters per FR.

Parameter	**FR1**	**FR3**	**FR2**
Frequency [GHz]	3.775	15.0	27.1
Duplex	TDD	TDD	TDD
Bandwidth [MHz]	50	200	400 (UL) / 800 (DL)
N_{CC} (UL / DL)	1	2	4 / 8
μ (SCS) [kHz]	1 (30)	2 (60)	3 (120)
Receiver array	1x1	2x2	4x4
Transmitter array	2x2	4x4	8x8
f_{scaling}	0.74[a]	0.49	0.49[b]

[a] Derived from FR1 measurements conducted in [10].
[b] Derived from FR2 measurements conducted in [9].

In the case of FR2, this mapping is derived from measurements of [9]. The corresponding logs contain UE-reported Key Performance Indicators (KPIs), such as received power and Channel Quality Indicator (CQI), as well as application-layer throughput measurements, which enables the determination of a device-specific relationship between radio conditions and achievable data rate. For FR1, measurement results from [10] are utilized, which provide the same set of metrics and thus allow the derivation of a comparable mapping approach. Since no specific measurements for FR3 are currently available in the considered industrial environment, the empirically obtained FR2 mapping is adopted for FR3 to account for the expected propagation behavior and comparable system design.

For each position of the mobile receiver, the simulated received power P_{rx} is first converted into a Signal-to-Interference-plus-Noise Ratio (SINR) value according to

$$\mathrm{SINR} = P_{\mathrm{rx}} - P_{\mathrm{noise}}, \qquad P_{\mathrm{noise}} = -174 + 10\log_{10}(B), \quad (1)$$

where B denotes the single-carrier bandwidth in Hz. The resulting SINR value is mapped to the highest admissible CQI index whose threshold is not exceeded. Independently of the considered frequency range, each CQI index i corresponds to a spectral efficiency η_i as specified in [13]. Based on this efficiency, the theoretical single-carrier PHY-layer peak data rate for CQI i is computed according to [14] as

$$R_{\mathrm{PHY},i} = 10^{-6} \cdot v_{\mathrm{layers}} \cdot \eta_i \cdot \frac{12 \cdot N_{\mathrm{PRB}}}{T_s} \cdot (1 - \mathrm{OH}), \quad (2)$$

where v_{layers} denotes the number of Multiple Input Multiple Output (MIMO) layers, N_{PRB} the maximum number of physical resource blocks for the given bandwidth as well as numerology μ, $T_s = 10^{-3}/(14 \cdot 2^{\mu})$ the symbol duration, and OH the overhead fraction.

To account for implementation-specific and system-level losses, the scaling factor f_{scaling} is utilized. For FR1 and 2, the factor is derived from the measurement logs for each CQI level as

$$f_{\mathrm{scaling}} = \frac{R_{\mathrm{meas}} \;/\; N_{\mathrm{CC}}}{R_{\mathrm{PHY},i}}, \quad (3)$$

where R_{meas} denotes the measured throughput aggregated over all N_{CC} component carriers. This factor captures practical losses due to Time Division Duplex (TDD) duty cycle, scheduling inefficiencies, protocol overhead, and retransmissions. A weighted overall f_{scaling} is computed across all CQI levels and applied to all FRs, whereby the same value is used for FR3 as for FR2 (see Tab. I). Finally, the estimated data rate R_{est} is obtained as

$$R_{\mathrm{est}} = R_{\mathrm{PHY},i} \cdot N_{\mathrm{CC}} \cdot f_{\mathrm{scaling}}. \quad (4)$$

This procedure establishes a consistent link between simulated propagation conditions and realistic, device-specific throughput estimates, and is therefore utilized in this work to analyze the performance potential of each FR.

IV. Performance Evaluation Across FR1–FR3

This section presents the findings of the proposed simulation framework and resulting performance analysis. First, the accuracy of the frequency-dependent ray tracing computations is assessed through a comparison of predicted and measured Path Loss (PL). Subsequently, coverage and capacity trade-offs are analyzed in a large-scale indoor industrial environment. Finally, deployment scaling is investigated in a highly cluttered indoor scenario, evaluating the impact transmitter density on target coverage and achievable UE data rates.

A. Cross-frequency Calibrated FR1-3 Path Loss Prediction

The evaluation of the received power prediction for FR1 and FR2 is presented in Fig. 3 utilizing two complementary representations. First, the PL is analyzed as a function of 3D distance between the static transmitter and mobile receiver. The plot includes measured values, ray tracing simulation results, and predictions obtained from the considered channel models. Second, the absolute PL prediction error with respect to the measured values is assessed using the Empirical Cumulative Distribution Function (ECDF), providing a statistical characterization of the model accuracy.

As indicated by the 95 % confidence intervals, a range of path loss values can occur at a given 3D distance due to varying propagation conditions within the industrial environment under consideration. The intervals of simulated and measured values do not perfectly overlap, which can be attributed to discrepancies between the modeled and real-world environment, since not all objects and material properties can be perfectly captured. Nevertheless, the RMSE values reported in Tab. II, amounting to 3.11 dB for FR1 and 4.79 dB for FR2, demonstrate that the applied simulation calibration (cf. Fig. 2) substantially improves the correlation between ray tracing simulations and measurement data. These results confirm that the calibrated framework reliably captures the propagation behavior in both FRs and can therefore be extrapolated to FR3, where a prediction error below 5 dB can be expected.

In contrast to the calibrated ray tracing results, the PL predictions obtained from the considered channel models exhibit substantially larger deviations from the measured values. As expected, these models provide only a generalized representation of the scenario-specific propagation conditions, resulting in RMSE values ranging from 8.38 dB to 26.01 dB (cf. Tab. II). Among the evaluated approaches, the Winner II B3 model achieves the highest accuracy, with an RMSE of 14.42 dB in FR1 and 8.38 dB in FR2. This can be attributed to its underlying scenario assumptions, which closely resemble the investigated environment: wide, but non-ubiquitous coverage,

TABLE II: RMSE values of path loss models and ray tracing simulations compared to FR1 and FR2 measurements.

	FR1	FR2
Winner II A1	26.01 dB	23.57 dB
3GPP InF	18.20 dB	15.50 dB
Winner II B3	14.42 dB	8.38 dB
Ray tracing simulation	3.11 dB	4.79 dB

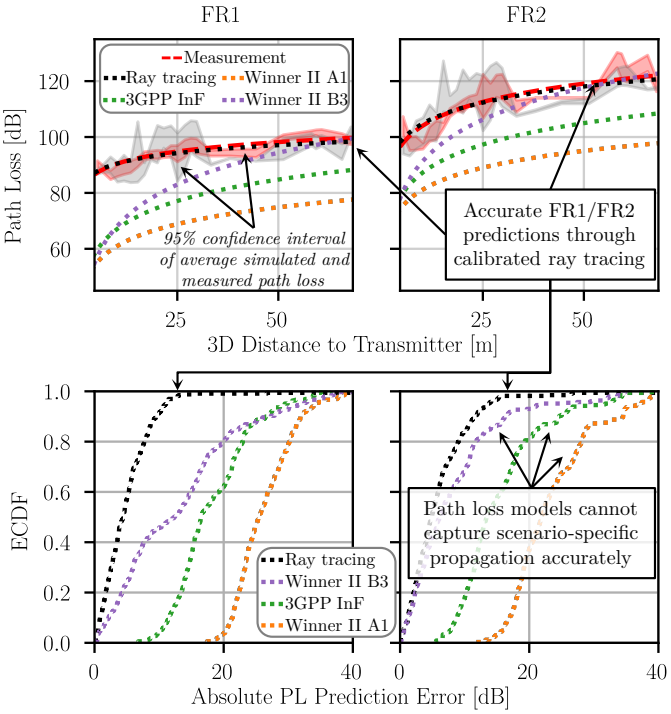

Fig. 3: Validation of path loss prediction by refined ray tracing simulations and various indoor channel models in comparison with FR1/FR2 measurements.

low mobility (< 5 km/h), large distances between transmitters and receivers, and both Line-of-Sight (LOS) and Non-Line-of-Sight (NLOS) conditions [11]. Despite the observed deviations, the predicted PL trends indicate that such models remain suitable for initial propagation assessments, particularly when only limited environmental and network information is available. For the subsequent analyses, however, the measurement-calibrated ray tracing framework is employed to simulate received power in each FR, ensuring scenario-specific and cross-frequency calibrated propagation evaluation.

B. Frequency-specific Performance and Coverage Trade-offs

To investigate the coverage and performance of the three FRs in the modeled indoor industry environment, Fig. 4 and Fig. 5 present Radio Environmental Maps (REMs) of the simulated received power and estimated UL data rate, respectively. Clear differences can be observed in terms of spatial coverage and achievable performance.

For FR1, using the configuration parameters summarized in Tab. I, connectivity is maintained at 99.6 % of all evaluated receiver positions, demonstrating excellent coverage robustness across the industrial shop floor. However, the limited bandwidth constrains the attainable peak throughput, resulting in a maximum UL data rate of 41.56 Mbit/s. Since NLOS conditions barely affect FR1 connectivity, this throughput can be sustained across the mobile UE's trajectory.

A different behavior is observed for FR2 at 27.1 GHz. At this frequency, received power values decrease significantly, particularly in NLOS conditions, which results in disconnections, as reflected in the estimated UL data rate shown in Fig. 5. Although the maximum UL data rate reaches

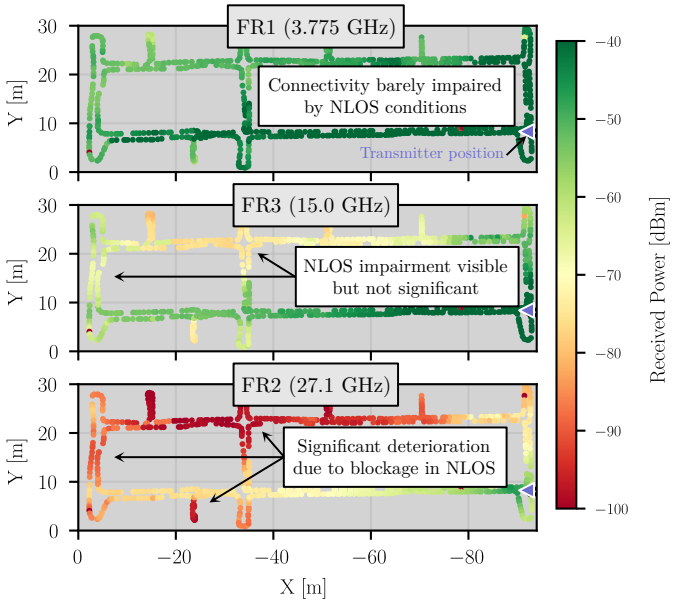

Fig. 4: Results of calibrated ray tracing simulations for FR1-3 in large-scale industrial environment visualizes radio propagation characteristics.

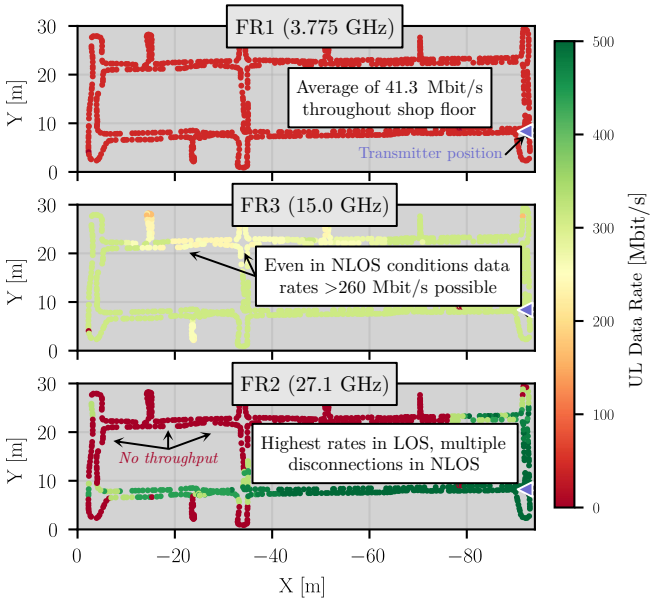

Fig. 5: Frequency-dependent performance prediction for mobile UE highlights the balance between link stability and performance in FR3.

623.96 Mbit/s, the average throughput across the shop floor is comparatively low at 244.64 Mbit/s, since only 49.4 % of receiver locations remain connected, revealing substantial outage regions caused by the blockage sensitivity of FR2.

Positioned between these two extremes, FR3 at 15.0 GHz also shows a visible impact of LOS blockage in the received power values, though considerably less severe than in FR2. The achievable performance is characterized by a maximum UL data rate of 311.98 Mbit/s and an average of 293.98 Mbit/s. While providing substantially higher throughput than FR1, connectivity is maintained at 99.4 % of UE positions, which is comparable to FR1 and superior to FR2. This highlights the balanced propagation characteristics and performance capabilities of the upper mid-band.

Overall, FR1 ensures highly stable coverage but remains bandwidth-limited, whereas FR2 delivers exceptional peak rates at the expense of spatial robustness. FR3, by contrast, emerges as a highly effective alternative, enabling high data rates while maintaining a low outage probability.

C. Deployment Scaling in Cluttered Indoor Environments

While the previous study compared link stability and performance of the considered FRs under identical deployment conditions, the following experiment investigates how increasing transmitter density affects coverage and achievable data rates in a highly cluttered indoor environment. For this purpose, a dedicated logistics warehouse scenario is modeled, as depicted in Fig. 6a. The environment consists of four double shelf rows with five levels each and a total height of 5.4 m. The shelf stock level is varied between 10 %, 50 %, and 90 % to model different degrees of environmental clutter and their impact on radio propagation and necessary infrastructure density.

To ensure a fair comparison across all FRs under their respective configurations, the *target coverage* is evaluated based on achieving at least 99 % of the configuration-dependent maximum UL data rate. Accordingly, throughput thresholds of 41.14 Mbit/s, 617.72 Mbit/s, and 308.86 Mbit/s are obtained for FR1, 2, and 3, respectively. For each stock level and FR, Fig. 6b reports the percentage of prioritized floor area satisfying this criterion (target coverage) as well as the average UL data rate of the mobile UE as the number of transmitters increases from one to ten. The considered setup represents a distributed antenna system, where the transmitter density is gradually increased to improve spatial coverage while keeping the overall system capacity unchanged. For each transmitter count, the combination yielding the maximum achievable coverage among the ten predefined candidate positions is selected.

At a stock level of 10 %, only one FR1 transmitter is needed to reach a target coverage of over 70 %. Even when increasing clutter to 50 % or 90 %, only two transmitters are required to achieve comparable coverage, confirming the high robustness of FR1 in terms of coverage, although the achievable peak rate remains bandwidth-limited.

In contrast, sustaining 99 % of the maximum data rate across the prioritized area with FR2 requires substantially higher transmitter densities. Even with ten transmitters, the target coverage reaches only 83.3 %, 70.0 %, and 67.8 % for 10 %, 50 %, and 90 % stock level, respectively. Although FR2 provides the highest achievable throughput, its high blockage sensitivity results in dense infrastructure requirements.

In comparison, FR3 exhibits a balanced scaling behavior. Five combined transmitters lead to a target coverage of more than 95 % at 10 % stock level, rising to six at 50 % and eight at 90 %. Compared with FR1, the higher carrier frequency requires additional infrastructure, yet substantially greater peak rates are achieved. Relative to FR2, significantly fewer transmitters are needed to sustain 95 % of target coverage, indicating improved robustness to challenging radio conditions.

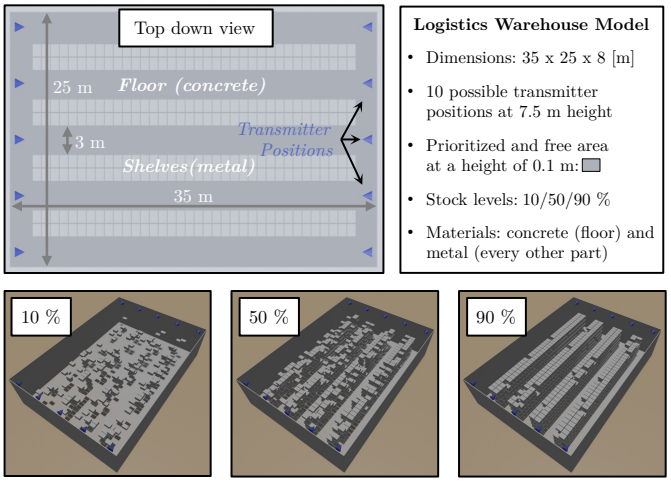

(a) Logistics warehouse scenario with varying stock levels

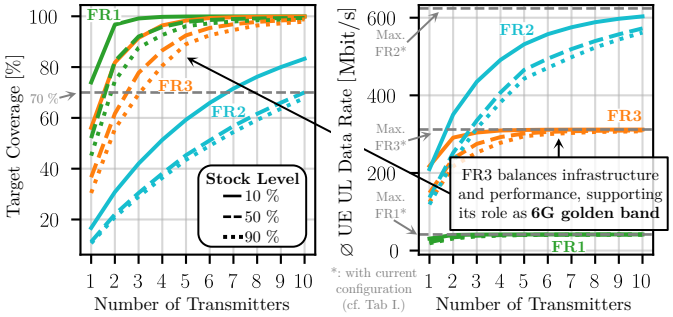

(b) Impact of transmitter density on coverage and UE performance

Fig. 6: Deployment scaling results in highly cluttered indoor environment, emphasizing the balanced deployment characteristics of FR3.

Summarized, FR1 offers infrastructure-efficient coverage with limited capacity, whereas FR2 provides superior peak performance at the expense of scalability in obstructed environments. In contrast, FR3 reconciles both dimensions ("*two birds with one stone*") by combining elevated throughput with moderate transmitter density requirements, which highlights FR3 as a compelling standalone solution. A quantitative summary of the experimental results is provided in Tab. III.

V. Conclusions and Outlook

This work presented a measurement-grounded framework for a systematic assessment of FR1, 2, and 3. By calibrating frequency-dependent ray tracing simulations using extensive measurements, a physically validated comparison across all three FRs is enabled, achieving a prediction accuracy with an RMSE between 3.11 dB and 4.79 dB. Furthermore, a device-specific mapping from received power to achievable data rate is developed, providing a consistent correlation between physical-layer results and system-level performance. The evaluation confirmed FR3 as promising deployment alternative, as it exhibits higher coverage as well as link stability than FR2 and offers increased capacity compared to FR1. Additionally, in a highly cluttered warehouse scenario, the results indicate that FR3 achieves the most favorable coverage–capacity trade-off by balancing infrastructure density and achievable UE throughput effectively. Overall, these findings reinforce FR3 as 6G *golden band*. However, comprehensive field trials and regulatory clarity regarding upper mid-band spectrum allocation will be essential to verify these advantages under real-world conditions and to ensure coexistence with pre-existing radio systems.

Future work will extend the analysis through channel emulator studies of dynamic orchestration strategies across FRs, integration of refined ray-tracing results into an open-source network simulator for system-level evaluations under diverse traffic models, and validation of the methodology in additional large-scale deployment environments.

TABLE III: Summary of evaluation metrics per FR.

Sec.	Parameter	FR1	FR3	FR2
IV-B	∅RP [dBm]	-43.26	-58.62	-81.73
	∅UL DR [Mbit/s]	41.35	**293.98**	244.64
IV-C	No. of Transmitters (70 % TC)	1	2	7
	∅UL DR (70 % TC) [Mbit/s]	30.76	291.05	575.38
	∅UL DR / Tx (70 % TC) [Mbit/s]	30.76	**145.52**	82.20

RP: Received Power; DR: Data Rate; TC: Target Coverage (10% stock level)

Acknowledgment

This work has been funded by the German Federal Ministry of Research, Technology and Space (BMFTR) in the course of the *VICTOR6G* project under grant no. 16KIS2549, the *6GEM+* Transfer Hub under grant no. 16KIS2412, and the *GEM-X* project under grant no. 16KISS005.

References

[1] Ericsson. Mobility report 11/2025. [Online]. Available: www.ericsson.com/en/reports-and-papers/mobility-report

[2] R. Tallat, A. Hawbani, X. Wang, A. Al-Dubai, L. Zhao *et al.*, "Navigating industry 5.0: A survey of key enabling technologies, trends, challenges, and opportunities," *IEEE Commun. Surv. Tutor.*, vol. 26, no. 2, 2024.

[3] A. Bazzi, R. Bomfin, M. Mezzavilla, S. Rangan, T. Rappaport *et al.*, "Upper mid-band spectrum for 6G: Vision, opportunity and challenges," *IEEE Communications Magazine*, vol. 64, no. 1, 2026.

[4] M. Ying, D. Shakya, T. S. Rappaport *et al.*, "Upper mid-band channel measurements and characterization at 6.75 GHz FR1(C) and 16.95 GHz FR3 in an indoor factory scenario," in *Proc. IEEE ICC*, 2025.

[5] D. Shakya, M. Ying, T. S. Rappaport *et al.*, "Comprehensive FR1(C) and FR3 lower and upper mid-band propagation and material penetration loss measurements and channel models in indoor environment for 5G and 6G," *IEEE Open J. Commun. Soc.*, vol. 5, 2024.

[6] S. Kang, M. Mezzavilla, S. Rangan, A. Madanayake, S. B. Venkatakrishnan *et al.*, "Cellular wireless networks in the upper mid-band," *IEEE Open J. Commun. Soc.*, vol. 5, 2024.

[7] Z. Cui, P. Zhang, and S. Pollin, "6G wireless communications in 7–24 GHz band: Opportunities, techniques, and challenges," in *Proc. IEEE DySPAN*, 2025.

[8] 3GPP Technical Report (TR) 38.901 V19.2.0, "TSG radio access network; study on channel model for frequencies from 0.5 to 100 GHz (release 19)," 2025.

[9] M. Danger, C. Arendt, H. Schippers, S. Böcker, N. Beckmann *et al.*, "6G industrial networks: Mobility-centric evaluation of multi-cell mmWave systems," in *Proc. IEEE VTC-Spring Conf.*, 2025.

[10] C. Arendt, S. Böcker, C. Bektas, and C. Wietfeld, "Better safe than sorry: Distributed testbed for performance evaluation of private networks," in *Proc. IEEE FNWF Conf.*, Oct. 2022.

[11] P. Kyösti, J. Meinilä, L. Hentilä, X. Zhao, T. Jämsä *et al.*, "WINNER II channel models," IST-WINNER, Deliverable D1.1.2 V1.2, 2007.

[12] J. Hoydis, S. Cammerer, F. Ait Aoudia, M. Nimier-David, L. Maggi *et al.*, "Sionna," 2022, https://nvlabs.github.io/sionna/.

[13] 3GPP Technical Specification (TS) 38.214 V18.8.0, "TSG radio access network; nr; physical layer procedures for data (release 18)," 2025.

[14] 3GPP Technical Specification (TS) 38.306 V18.8.0, "TSG radio access network; nr; user equipment radio access capabilities (release 18)," 2025.